

Short range order structure of amorphous B₄C boron carbide thin films

Ruqiang Bao · Douglas B. Chrisey

Received: 18 October 2010 / Accepted: 21 January 2011 / Published online: 11 February 2011
© Springer Science+Business Media, LLC 2011

Abstract B₄C boron carbide thin films deposited by radio frequency magnetron sputtering in the temperature ranging from room temperature to 650 °C are amorphous. In this article, pair distribution function (PDF) and Fourier transform infrared (FTIR) spectroscopy were used to characterize the short range order (SRO) structure of amorphous B₄C thin films. FTIR spectra indicated that icosahedrons exist in the amorphous B₄C thin films. The existence of icosahedrons was further verified by the PDFs of amorphous B₄C thin films, which were derived from digital selected area electron diffraction patterns. Furthermore, by comparing the PDFs of amorphous B₄C thin films with those of three crystalline boron modifications and three structural models of boron carbides (B₄C or B₁₀C₂), the SRO structure of amorphous B₄C thin film was revealed to be similar to that of β -rhombohedral boron, but with the peak shifted to shorter distance.

Introduction

Boron carbide is one of the well-known hardest materials [1–3] as well as a semiconductor with a bandgap dependent on many factors including the boron to carbon stoichiometry [4, 5]. Because of the unique electronic properties and the unusual quality of self-healing of radiation damage [6, 7], boron carbide-based semiconductors have drawn attentions recently for power harvesting and sensing applications, such as photovoltaic devices [8], beta-voltaic

devices [7], and neutron detectors [9–12]. Boron carbide thin films have been prepared by different techniques, such as chemical vapor deposition [13–15], magnetron sputtering [2, 3, 16, 17], pulsed laser deposition [18–20], and ion beam synthesis [21]. Due to boron carbide's high melting point (2450 °C) [22], boron carbide thin films deposited at room temperature or relatively low temperatures are amorphous and only show crystallinity starting from 950 °C [16]. However, there has hitherto been no further effort to characterize the short range order (SRO) structure of amorphous boron carbide and correlate the structure with the properties. This is partially due to the fact that boron carbide is a low atomic number (Z) alloy and has a complex structure. Therefore, the local structure determination for amorphous boron carbide is quite difficult. The SRO structure of amorphous materials is commonly investigated by X-ray diffraction (XRD), from which the radial distribution function and the pair distribution function (PDF) can be derived. However, the low Z materials have low X-ray atomic scattering factors. So, the scattered X-ray intensity is too weak to be used to determine the SRO of amorphous boron carbide thin films (several hundreds of nm in thickness). The complex structure of crystalline boron-rich solid materials comes from their basic structural unit, i.e., the distorted icosahedron, and the number of atoms in the unit cell. The former causes the bond length to be distributed over a wide range. The latter ranges from 12 for α -rhombohedral boron to 1608 for YB₆₆ type crystal [5].

The understanding of the SRO structure of amorphous boron carbide thin films is key in exploring applications of boron carbide materials as semiconductors in extreme environments. An application of boron carbide to fabricate beta- and alpha-voltaic devices for nuclear batteries is based on its extreme radiation hardness, i.e., the self-healing of

R. Bao · D. B. Chrisey (✉)
Department of Materials Science and Engineering,
Rensselaer Polytechnic Institute, MRC 142, 110 8th Street,
Troy, NY 12180, USA
e-mail: chrisd@rpi.edu

radiation-induced damage [7]. The extreme radiation hardness results from the icosahedral structural unit found in boron-rich solid materials. The formation of such structure is due to the electron-deficient bonding within the boron-rich solids. A regular icosahedron, schematically shown in Fig. 1, is a 12-atom cluster in which 12 boron atoms occupy the 12 vertices. The radiation-induced damage is caused by energetic particle bombardment which displaces the atoms in the solid from their original lattice sites and introduces defects like vacancies and interstitials. According to Carrard et al.'s research [6], the absence of radiation-induced damage in icosahedral boron-rich solids is ascribed to the fast recombination of the radiation-induced defects. It has been suggested that if boron atoms are displaced from the icosahedrons as interstitials, the boron interstitials have positive charges and the corresponding icosahedrons with boron vacancies are associated with negative charges. The self-healing of radiation-induced damage has been suggested to be driven by Coulomb attractions between the positively charged boron interstitial ions, B^+ , and the regions of increased negative charges associated with boron vacancies [6]. Moreover, the very small size of a boron cation aids its diffusion and thereby facilitates the recombination. However, in an amorphous boron carbide thin film, it is not clear if the icosahedron is still its basic structural unit. It was reported that the types of charge carriers in an amorphous boron carbide thin film can be controlled by modifying local physical structure, which can alter semiconducting transport properties between p-type and n-type [8]. Without an understanding of SRO structure of amorphous boron carbide thin films, this unique transportation characteristic cannot be understood clearly.

By analyzing electron diffraction patterns of amorphous boron carbide thin films, it becomes approachable to characterize the SRO structure. In this study, electron

diffraction patterns were used instead of XRD patterns, because the electron atomic scattering factors for low Z materials are much larger than X-ray atomic scattering factors. In addition, typical electron diffraction intensities are $\sim 10^8$ times larger than XRD intensities. In comparison, the structures of several conventional crystalline boron modifications (α -rhombohedral boron, β -rhombohedral boron, and tetragonal boron) and boron carbides were built based on the data in the literatures or by first principles. The PDFs for these crystals were extracted from the volume of $\sim 10^5$ atoms based on the built structures. Fourier transform infrared (FTIR) spectroscopy was also used to help identify the structural motif of amorphous B_4C thin films. Our analysis showed that icosahedrons exist in the amorphous B_4C thin films and the SRO structure of the films is similar to that of β -rhombohedral boron, but with the peak shifted to the shorter distance.

Experimental details

Amorphous B_4C thin films were deposited at room temperature (RT), 350, 500, and 650 °C on polished single crystal quartz (0001) or double-side polished KBr substrates by radio frequency magnetron sputtering from a polycrystalline B_4C target (99.5% in purity) at a working pressure of 5 mTorr Ar. The input power is 200 W. All substrates were preheated at the target temperature for 30 min before deposition. Prior to deposition, sputter cleaning was performed to eliminate the native oxide of the target and clean the surface of quartz substrates. B_4C thin films (~ 60 nm in thickness) deposited on quartz substrates were lifted off in distilled water for high resolution transmission electron microscopy (HRTEM) experiments on JEOL 2010 with an acceleration voltage of 200 kV. These thin samples were prepared to reduce the inelastic scattering and the plural scattering by keeping the ratio of the intensity under the zero-loss peak to the intensity in the low-loss portion of the electron energy loss spectrum to be less than 10%. Selected area electron diffraction (SAED) pattern was digitally recorded by Gatan Dualvision camera (Model 780). The camera length was calibrated using single crystal silicon. HRTEM image was recorded using GIF camera (794IF). A Gatan 695 parallel electron energy loss spectrometer (PEELS) was also used for microanalysis. The samples for FTIR were B_4C thin films (200 nm in thickness) deposited on optical grade KBr substrates, which were chosen because FTIR spectra could be collected with the weak background signal for wavenumber greater than 450 cm^{-1} . FTIR was conducted on a Perkin Elmer Spectrum One FT-IR spectrometer with 64 scanned interferograms to reduce noise.

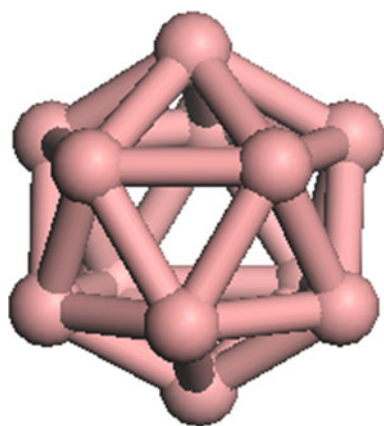


Fig. 1 The schematic structure of a regular B_{12} icosahedron

Pair distribution function

The reduced scattering intensity for amorphous alloys, derived by Cockayne et al. [23, 24], is given by

$$\varphi(s) = \frac{[I(s) - N\langle f^2 \rangle]s}{N\langle f \rangle^2} \quad (1)$$

where $\langle f \rangle^2 = (\sum_m N_i f_i)^2 / N^2$, $\langle f^2 \rangle = (\sum_m N_i f_i^2) / N$, $N = \sum_m N_i$, f_i is the atomic scattering factor of atom type i , m is the number of atom type (in the case of boron carbide, $m = 2$), N is the total number of atoms, N_i is the number of atoms of type i , $I(s)$ is the scattering intensity normalized to the intensity scattered by an electron without considering the small angle scattering, and s is the scattering vector defined as $2(\sin\theta)/\lambda$ (λ is the wavelength of incident radiation and θ is the scattering angle). Fourier inversion of Eq. 1 yields the reduced radial distribution function

$$G(r) = 8\pi \int_0^\infty \varphi(s) \sin(2\pi rs) ds \quad (2)$$

where r is the distance from arbitrary origin. The PDF is obtained by

$$g(r) = \frac{G(r)}{4\pi r \rho_0} + 1 \quad (3)$$

where ρ_0 is the average density of all atom types.

MATLAB® software (Mathworks, Inc) was used to read out the scattering intensity from digital SAED micrograph for amorphous B_4C thin film by simply taking radial line scan of the diffraction pattern starting from the sharp central spot because of the circular symmetry of electron diffraction pattern. The scattering intensity was then smoothed by adjacent average after removing background. Electron atomic scattering factors of boron and carbon atoms were obtained from the literature [25], and the $\langle f \rangle^2$ and $\langle f^2 \rangle$ were

calculated according to the definition in this work. An approximate value of N was obtained by matching Nf^2 to $I(s)$ at large s with N as a variable parameter. Subsequently, Eqs. 1 and 2 were used to form the reduced scattering intensity $\varphi(s)$ and the reduced radial distribution function $G(r)$, respectively. The procedure was repeated for a slightly different value of N , and an optimum N was obtained by minimizing oscillations in $G(r)$ for small r . Finally, Eq. 3 was used to yield the PDF.

The PDFs of crystalline boron and boron carbide were obtained through the built structural models. The structural models of three crystalline boron modifications, i.e., α -rhombohedral boron, β -rhombohedral boron, and tetragonal (T50) boron, were built according to the data in the literatures [26], [27], and [28], respectively. They are shown in Fig. 2a, d, and e, respectively. Two structural models, $B_{11}C_p(C-B-C)$ and $B_{11}C_e(C-B-C)$, for B_4C boron carbide were built by adding three atoms (C–B–C) linear chain along the main diagonal and replacing one boron atom by one carbon atom at the polar site and at the equatorial site of icosahedrons, respectively, on the basis of the structural model of α -rhombohedral boron. Here, the part of outside bracket indicates the structure of the icosahedron and the part in the bracket represents the structure of linear chain. The subscript number represents the number of atoms in the icosahedron and the subscript letter represents the position of atoms in the icosahedron. The p represents the polar site and the e represents the equatorial site in the icosahedron. More details are available in the later section. Figure 2b shows the structure of $B_{11}C_p(C-B-C)$. The unit cell parameters for these two models were obtained from the literature [29]. The structure of $B_{11}C_p(C-B-C)$ was reported to be the most stable for crystalline B_4C boron carbide [30]. Structural model of boron carbide with the composition of $B_{10}C_2$, as shown in Fig. 2(c), was also built by replacing one boron atom at the polar site and the other at the equatorial site of icosahedron, respectively, by two

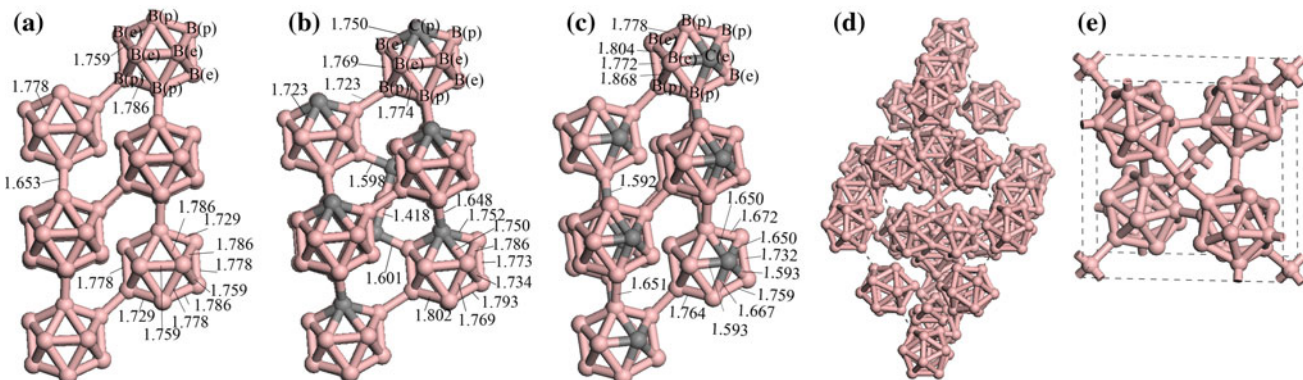


Fig. 2 The structural models for **a** α -rhombohedral boron, **b** $B_{11}C_p(C-B-C)$, **c** $B_{10}C_2$, **d** β -rhombohedral boron, and **e** tetragonal boron (T50 boron). Some bond lengths are labeled in the unit of Å

carbon atoms on the basis of the structure of α -rhombohedral boron. The geometry optimization and structural relaxations were then performed for these three structural models of boron carbide by using the Broyden–Fletcher–Goldfarb–Shanno method [31] with the variable cell method of fixed basis quality to minimize the total energy. The total energy calculations were performed by using nonlocal corrected generalized gradient approximation based on the most popular Perdew–Burke–Ernzerhof formulation [32]. Pseudoatomic calculations were performed for B 2s, 2p and C 2s, 2p shells. The convergence conditions were the total energy convergence tolerance of 10^{-5} eV/atom, the maximum force tolerance of 0.03 eV/ \AA , the maximum displacement tolerance of 0.001 \AA , and the maximum stress component tolerance of 0.05 GPa. Finally, the PDFs of these crystalline borons and boron carbides were extracted from a volume of $\sim 10^5$ atoms based on these models.

Results and discussion

Figure 3 shows the HRTEM images and SAED patterns for B_4C thin films deposited at 500 and 650 °C, which are similar to those for the films deposited at RT and 350 °C shown in [17]. The disordered lattice images and diffuse halos in the SAED patterns for all films reveal that the

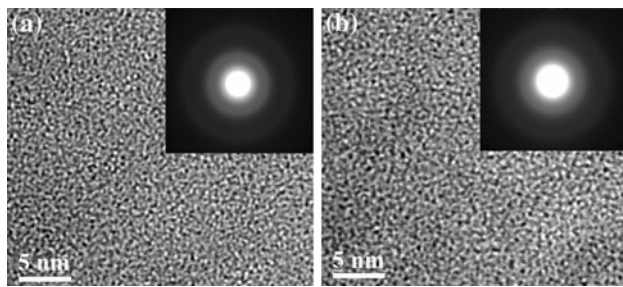


Fig. 3 HRTEM images of amorphous B_4C thin films deposited at **a** 500 °C and **b** 650 °C. The insets show the corresponding SAED patterns of the films

Table 1 The positions of the maxima in $I(s)$ for amorphous boron and boron carbide measured by electron diffraction (\AA^{-1})

Amorphous boron				Amorphous B_4C deposited at 350 °C(this study)	
PVD		CVD			
Katada [34]	Palatnik et al. [35]	Galasso et al. [36, 37]	Kobayashi[33]	Sample B	Sample C
0.232	0.222	0.227	0.228	0.233	0.237
0.428	0.400	0.400	0.395	0.395	0.405
			0.578	0.562	
0.759	0.714	0.714	0.709	0.709	0.743

deposited B_4C thin films are amorphous. As an example, Fig. 4 shows the scattering intensity for B_4C thin film deposited at 350 °C. The scattering intensity is scattering vector dependent. Three peaks located at 0.237, 0.405, and 0.743 \AA^{-1} , respectively, can be identified and correspond to three diffuse halos in the SAED pattern of B_4C thin film deposited at 350 °C. Table 1 lists the positions of the maxima of diffraction intensity reported by previous literatures for amorphous boron by using electron beam diffraction as well as the data of amorphous B_4C thin film in this study. For comparison, all scattering vectors follow the same definition used in this article. It can be seen that the maxima positions of diffraction intensity for B_4C thin film deposited at 350 °C are similar to the reported data of amorphous boron, except the additional maxima position at $\sim 0.56 \text{\AA}^{-1}$ reported by Kobayashi [33]. The origin for the additional peak is not clear but it may be caused by different deposition method and condition. From Table 1, it can be seen that the corresponding scattering vector at the maxima position of B_4C thin film is larger than that of amorphous boron, except the data reported by Katada [34]. Figure 5 shows the reduced radial distribution functions and the PDFs of B_4C thin films deposited at different substrate temperatures. The results are similar for all thin films except that the peak positions shift a little bit for the

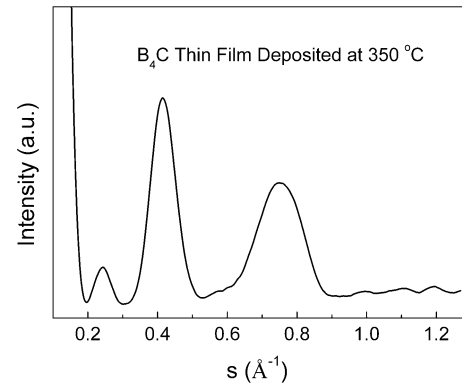
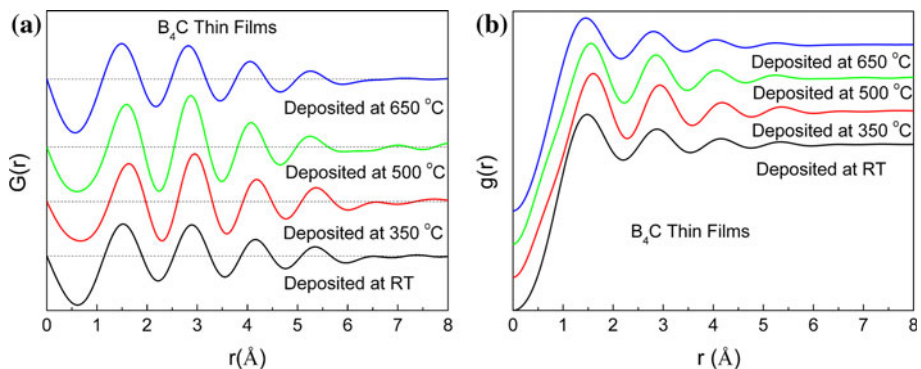


Fig. 4 The scattering intensity for amorphous B_4C thin film deposited at 350 °C

Fig. 5 **a** The reduced radial distribution functions and **b** PDFs of amorphous B_4C thin films deposited at different substrate temperatures



films deposited at different substrate temperatures. Taking the $g(r)$ of B_4C thin film deposited at 350 °C as an example, the first and the second peaks are located at 1.63 and 2.95 Å, respectively. The former is close to the first nearest distance and the latter close to the second nearest distance in the icosahedron which will be discussed in detail in the following discussions.

Figure 6 shows the FTIR spectra of amorphous B_4C thin films. The spikes come from the substrate. It can be seen that the FTIR spectra of amorphous B_4C thin films only show a strong and broad peak at $\sim 1080 \text{ cm}^{-1}$. FTIR spectrum for single crystal B_4C boron carbide has two strong absorption peaks: one located at $\sim 1080 \text{ cm}^{-1}$ and the other at $\sim 1600 \text{ cm}^{-1}$ [38]. The former peak is believed to be contributed by anti-symmetric stretching of icosahedrons and the latter is caused by anti-symmetric stretching of chain in crystalline B_4C boron carbide [39, 40]. Therefore, the fact that there is only one broad peak near 1080 cm^{-1} indicates the existence of icosahedrons in amorphous B_4C thin films.

Before discussing the structure of amorphous B_4C thin films, it is necessary to describe the structures of crystalline boron and boron carbide. In crystalline boron-rich solid materials, the B_{12} icosahedron plays an important role in the formation of the frameworks. The B–B bond length in the

regular icosahedron is 1.78 Å [34]. It is the distorted icosahedron instead of the regular icosahedron that exists in crystalline boron-rich solid materials, because by Jahn-Teller effect the reduction of the point group I_h of the regular B_{12} icosahedron to the subgroup D_{3d} (equivalent to space group $R\bar{3}m$) of the distorted icosahedron minimizes the total energy of the crystals [41]. Therefore, there are two types of equivalent sites in the icosahedron for α -rhombohedral boron: the polar site and the equatorial site, as labeled in Fig. 2a. Some of B–B bond lengths in the distorted icosahedrons are also shown. It can be seen that the B–B bond length in the distorted icosahedron is not a single value anymore due to the formation of different bonds: the intericosahedral bond, the intra-icosahedral bond, and the Δ -bond (three-center bond). The structure of β -rhombohedral boron is more complicated. There are 105 atoms in the unit cell, as shown in Fig. 2d. Crystal lattice of β -rhombohedral boron can also be described to be formed by B_{84} clusters. A cubic close package of the B_{84} clusters produces a rhombohedral unit cell with 105 atoms inside it. As shown in Fig. 7a, a B_{84} cluster is a building block of β -rhombohedral boron with a C_{60} -like surface built around a B_{12} icosahedron. In addition, there are two B_{28} clusters in the unit cell which are formed by fusing three distorted icosahedrons via face-to-face and linked together by an isolated boron atom, as shown in Fig. 7b. For tetragonal boron, there are four distorted icosahedrons and two isolated boron atoms, which link the icosahedrons, in the unit cell as shown in Fig. 2e. Therefore, in crystalline boron, there are at least four ways to link the distorted icosahedrons. First, icosahedrons may link directly to each other by the B–B inter-icosahedral bond (bond length $\sim 1.65 \text{ \AA}$), which can be found in α -rhombohedral boron and β -rhombohedral boron. Second, they may link together by the Δ -bonds (bond length $\sim 2.00 \text{ \AA}$) formed by the boron atoms at the equatorial sites, which appear in α -rhombohedral boron. Third, they may link through isolated boron atom (bond length 1.60 Å) as found in the tetragonal boron. Forth, they may link via fusing icosahedrons by face-to-face, as shown in Fig. 7b and c, which can be found in β -rhombohedral boron and AlB_{12} compound [5].

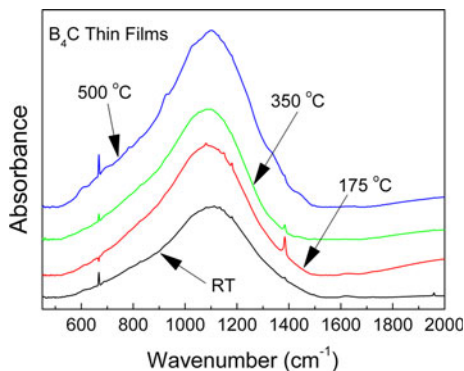
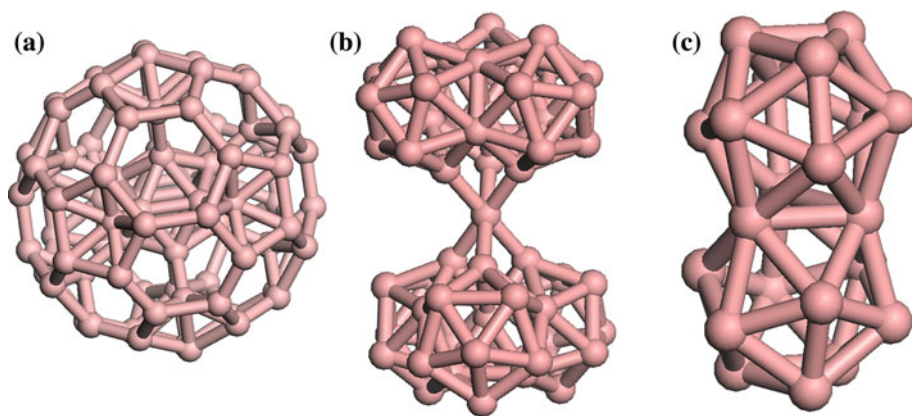


Fig. 6 FTIR spectra of amorphous B_4C thin films deposited at different substrate temperatures

Fig. 7 **a** The B_{84} cluster, **b** $B_{28}-B-B_{28}$ cluster, and **c** B_{21} cluster in β -rhombohedral boron or AlB_{12} compound



The ideal structure of crystalline B_4C boron carbide is believed to be based on an arrangement of distorted icosahedrons located at each vertex and three-atomic linear chains on the main diagonal of a rhombohedral Bravais lattice (space group $R\bar{3}m$). However, no experimental determination of the real atomic structure of crystalline B_4C boron carbide has been reported. The neutron scattering lengths of ^{11}B from ^{12}C are too close so that they cannot be distinguished from each other [42]. Although XRD allows the identification of a C–B–C chain, the location of the remaining C atom in the $B_{11}C$ icosahedron remains unclear because of the very similar X-ray atomic scattering factors of boron and carbon atoms. Moreover, Werheit [43] proposed that the composition range of boron carbide extends from $B_{4.3}C$ at the carbon-rich limit to $B_{\sim 11}C$ for the boron-rich solids by partial substitution of boron atoms both in the chains and in the icosahedrons by carbon atoms. Both the concentration of vacancies and the position of carbon atoms change with the composition of crystalline boron carbide. It is believed that, for B_4C (or $B_{12}C_3$), the different icosahedral-based (B_{12} and $B_{11}C$) and chain-based (C–B–C, C–B–B, C–□–C (□, vacancy), B–□–B, and C–C–C) structures form different elementary cells, which are statistically distributed over the whole structure [43]. Therefore, no unit cell can represent the whole structure as commonly found in conventional crystalline solids. By comparing existing infrared absorption and Raman diffusion measurements with the predictions of accurate ab initio lattice dynamical calculations performed for different structural models, Lazzari et al. [30] suggested that the ideal atomic structure of B_4C could be expressed as $B_{11}C_p(C-B-C)$, i.e., one icosahedron ($B_{11}C$) with the carbon atom staying at a polar site and a linear chain (C–B–C). By comparing the enthalpy of several structural models based on simulations from first principles, it is found that $B_{11}C_p(C-B-C)$ has the lowest energy [44]. But it should be noted that the difference of the average enthalpy among all structural models of boron carbide with the stoichiometry of B_4C is very small, especially between $B_{11}C_p(C-B-C)$

and $B_{11}C_e(C-B-C)$. As a result, it is possible that several structural models of B_4C boron carbide co-exist in real boron carbide materials [44]. Therefore, the PDFs of $B_{11}C_p(C-B-C)$ and $B_{11}C_e(C-B-C)$ are used as the references to study the structure of amorphous B_4C thin films. In addition, $B_{10}C_2$ is also used as a reference to study the effect of random occupation of carbon atoms on the structure of amorphous B_4C thin films.

Figure 2b shows the types of positions, labeled in the bracket, of carbon (gray ball) and boron (pink ball) atoms in the distorted icosahedron and some bond lengths in $B_{11}C_p(C-B-C)$. It can be seen that the shortest bond length (1.418 Å) in $B_{11}C_p(C-B-C)$ can be assigned to the C–B bond in the C–B–C chain but the longest bond length (1.802 Å) is given to the B–B bond in the distorted icosahedron. When a carbon atom is at the end of the linear chain and a boron atom at the equatorial site of icosahedron, the C–B bond length is about 1.60 Å. Compared with the corresponding bond length in α -rhombohedral boron as shown in Fig. 2(a), some bond lengths in the icosahedron are changed due to the addition of carbon atoms. The C–B inter-icosahedral bond becomes shorter due to the carbon atoms at the polar site of icosahedrons. More significant change can be observed for both intra- and inter-icosahedral bond lengths in $B_{10}C_2$ by replacing two boron atoms with two carbon atoms, as shown in Fig. 2c. Therefore, the C–B bond length in boron carbide is shorter than the corresponding B–B bond length in α -rhombohedral boron, i.e., the C–B intra-icosahedral bond length is shorter than the B–B intra-icosahedral bond length and the C–B inter-icosahedral bond length is shorter than the B–B inter-icosahedral bond length.

Figure 8 shows the PDFs of the structural models for crystalline boron, crystalline boron carbide, and amorphous B_4C thin film deposited at 350 °C. The $g(r)$ of α -rhombohedral boron shows discrete peaks when the distance (r) is smaller than ~6 Å because of its relative simple structure. In other cases, the $g(r)$ shows discrete peaks only when the distance is smaller than ~3 Å. The three peaks in the first

peak package of the $g(r)$ of $B_{11}C_p(C-B-C)$ indicate three kinds of bonds, i.e., the C–B bond in the C–B–C chain, the C–B bond (where the carbon atom is at the end of C–B–C chain and the boron atom is at the equatorial site of icosahedron), and the intra-icosahedral bond. The replacement of two boron atoms in α -rhombohedral boron by two carbon atoms leads to three peaks in the first peak package of $B_{10}C_2$. As indicated by the PDF of β -rhombohedral boron, it is not surprising that β -rhombohedral boron was said to be like an amorphous material [4] because of the large unit cell, compared to the inter-atomic distances and its complex structure [27].

The arrangement of the distorted icosahedrons is quite random in the amorphous B_4C thin film. A three-dimensional random network built up in the aforementioned manners for crystalline boron extends over the whole film, which gives the diffuse halos of the electron diffraction pattern. The carbon atoms can replace the boron atoms randomly. Several articles [33–35, 45] reported the SRO structure of amorphous boron using the PDFs obtained through electron diffraction and XRD techniques. However, although all reports proposed the existence and the random arrangement of the B_{12} icosahedron, there was no agreement on the SRO structure of amorphous boron. For example, the structure of amorphous boron was suggested to be a frozen stage in the transition from α -rhombohedral to β -rhombohedral boron [45]; the arrangement of the B_{12} icosahedron was considered to be close to that of tetragonal boron [35]; and the SRO structure of amorphous boron was shown to be closer to that of the β -rhombohedral boron [33]. Comparing the peak shapes and positions of the $g(r)$ of B_4C thin film with those of crystalline boron and boron carbide, as shown in Fig. 8, the SRO structure of amorphous boron carbide seems to be close to that of $B_{11}C_p(C-B-C)$. However, some peaks, such as the peak at point d, are missing. More careful observation suggests that the peak shapes and positions of the $g(r)$ of B_4C thin film

are similar to those of β -rhombohedral boron, expect that the peak positions of B_4C thin film are shifted to shorter distance from those of β -rhombohedral boron, such as A, B, and C. Similar shift can be found in $B_{11}C_p(C-B-C)$ by comparing peak packages at A', B', and C', with those at A, B, and C, of β -rhombohedral boron, respectively. The shorter distance of B_4C thin film may be caused by the existence of carbon atoms and the random replacement of boron atoms by carbon atoms in the film. This can be easily understood by comparing the $g(r)$ of $B_{11}C_p(C-B-C)$ with that of $B_{11}C_e(C-B-C)$. The carbon atom at the polar site, instead of equatorial site, leads to the shorter C–B bond lengths, as indicated by the first sharp peak of the PDFs of these two structural models. The replacement of the boron atoms in α -rhombohedral boron by the carbon atoms also leads to the shorter C–B bond lengths, as indicated by first peak of the $g(r)$ of crystalline $B_{10}C_2$. Moreover, the residual internal stress is compressive and can be as large as ~ 3 GPa [2]. The large residual internal stress could further shorten the bond length. Furthermore, the oxidation of the film can shorten the bond length as well because the B–O bond length in amorphous tetrahedral BO_4 is 1.48 \AA [34]. But there is no detectable oxygen signal for the PEELS spectra of B_4C thin films, as shown in Fig. 9. The X-ray photoelectron spectroscopy analysis of amorphous B_4C thin films shows that the thickness of boron–carbon–oxygen layer is about 1 nm, which formed upon exposure to air [17]. Considering the thickness ($\sim 60 \text{ nm}$) of B_4C thin films, the influence of boron–carbon–oxygen layer on the bond length of thin film is negligible. Therefore, the SRO structure of amorphous B_4C thin films is similar to that of β -rhombohedral boron, but the peaks shift to shorter distance.

It should be noted that there are B_{84} and B_{28} –B–B₂₈ clusters in crystalline β -rhombohedral boron. In the latter case, the B_{28} is formed by fusing three icosahedrons. Because the SRO structure of amorphous B_4C thin films is

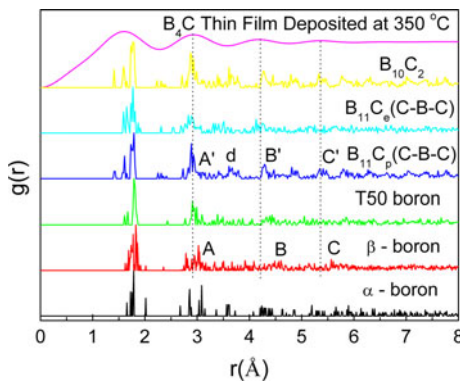


Fig. 8 The PDFs of several structural models of crystalline boron, crystalline boron carbide, and amorphous B_4C thin film deposited at $350 \text{ }^\circ\text{C}$

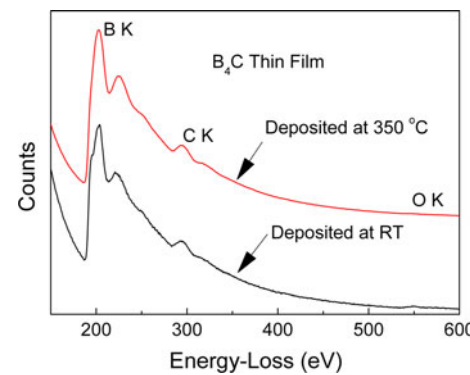


Fig. 9 PEELS spectra of amorphous B_4C thin films deposited at RT and $350 \text{ }^\circ\text{C}$

similar to the structure of β -rhombohedral boron, it is highly possible that B_{28} clusters exist in amorphous B_4C thin films. It is reasonable to infer that there are B_{21} clusters as well in amorphous B_4C thin films, which exist in AlB_{12} compound [5] and are constructed by fusing two icosahedrons via face to face. Although Cockayne [23, 24] suggested that the $G(r)$ can be used to determine atom types by deconvolution when there is a small degree of overlap of bond length, it is not applicable to amorphous B_4C thin films because of two obvious reasons: (1) the B–B and B–C bond lengths cover a large range and overlap each other and (2) the electron atomic scattering factors of boron and carbon atoms are very close to each other [25]. In addition, the peak position shift of the $g(r)$ of amorphous B_4C thin films deposited at different temperatures may be caused by the substrate temperature, which affects the growth mode and the surface mobility of adatoms. Further investigation is needed to study the peak shift.

Conclusion

B_4C thin films are amorphous when deposited by RF magnetron sputtering in the range of room temperature to 650 °C. Pair distribution function and FTIR were used to analyze the SRO structure of amorphous B_4C thin films. FTIR spectra indicated that icosahedrons exist in the amorphous B_4C thin films. Pair distribution functions of amorphous B_4C thin films were derived from digital SAED pattern of electron diffraction. By comparing PDFs of amorphous B_4C thin films with those of three crystalline boron modifications (α -rhombohedral boron, β -rhombohedral boron, and tetragonal boron) and three structural models of boron carbides ($B_{11}C_p(C-B-C)$, $B_{11}C_e(C-B-C)$, and $B_{10}C_2$), the SRO structure of amorphous B_4C thin film is found to be similar to that of β -rhombohedral boron but the peaks shift to the shorter distance. The peak shift could be caused by the existence of carbon atoms in the thin film and the random replacement of the boron atoms by the carbon atoms in the three dimensional network of the distorted icosahedrons.

Acknowledgement The authors would express their thanks to Prof. Pawel Kebinski at Rensselaer Polytechnic Institute for useful discussion and suggestions about the calculation of the reduced radial distribution function and pair distribution function. This study was supported by the DARPA Micro-Isotope Power Sources Program and Rensselaer Polytechnic Institute start-up funds.

References

- Chen MW, McCauley JW, Hemker KJ (2003) Science 299(5612):1563
- Wu ML, Kiely JD, Klemmer T, Hsia YT, Howard K (2004) Thin Solid Films 449(1–2):120
- Jacobsohn LG, Nastasi M (2005) Surf Coat Tech 200(5–6):1472
- Golikova OA (1979) Phys Status Solidi A 51(1):11
- Schmeichel R, Werheit H (1999) J Phys Condens Matter 11(35):6803
- Carrard M, Emin D, Zuppiroli L (1995) Phys Rev B 51(17):11270
- Emin D (2006) J Solid State Chem 179(9):2791
- Caruso AN, Billa RB, Balaz S, Brand JI, Dowben PA (2004) J Phys Condens Matter 16(10):L139
- Hong NN, Mullins J, Foreman K, Adenwalla S (2010) J Phys D 43(27):275101
- Osberg K, Schemm N, Balkir S, Brand JO, Hallbeck MS, Dowben PA, Hoffman MW (2006) IEEE Sens J 6(6):1531
- Day E, Diaz MJ, Adenwalla S (2006) J Phys D 39(14):2920
- Caruso AN, Dowben PA, Balkir S, Schemm N, Osberg K, Fairchild RW, Flores OB, Balaz S, Harken AD, Robertson BW, Brand JI (2006) Mater Sci Eng B 135(2):129
- Sezer AO, Brand JI (2001) Mater Sci Eng B 79(3):191
- Jansson U, Carlsson JO, Stridh B, Soderberg S, Olsson M (1989) Thin Solid Films 172(1):81
- Olsson M, Soderberg S, Stridh B, Jansson U, Carlsson JO (1989) Thin Solid Films 172(1):95
- Kulikovsky V, Vorlicek V, Bohac R, Ctvrtlik R, Stranyanek M, Dejneka A, Jastrabik L (2009) Diam Relat Mater 18(1):27
- Bao R, Chrisey DB (2010) Thin Solid Films 519(1):164
- Csako T, Budai J, Szorenyi T (2006) Appl Surf Sci 252(13):4707
- Kokai F, Taniwaki M, Takahashi K, Goto A, Ishihara M, Yamamoto K, Koga Y (2001) Diam Relat Mater 10(3–7):1412
- Kokai F, Taniwaki M, Ishihara M, Koga Y (2002) Appl Phys A 74(4):533
- Ronning C, Schwen D, Eyhusen S, Vetter U, Hofmann H (2002) Surf Coat Tech 158:382
- Suri AK, Subramanian C, Sonber JK, Murthy TSRC (2010) Int Mater Rev 55(1):4
- Cockayne DJH (2007) Annu Rev Mater Res 37:159
- Cockayne DJH, Mckenzie DR (1988) Acta Crystallogr A 44:870
- Doyle PA, Turner PS (1968) Acta Crystallogr A 24(3):390
- Decker BF, Kasper JS (1959) Acta Crystallogr 12(7):503
- Callmer B (1977) Acta Crystallogr B 33:1951
- Hoard JL, Hughes RE, Sands DE (1958) J Am Chem Soc 80(17):4507
- Aselage TL, Tissot RG (1992) J Am Ceram Soc 75(8):2207
- Lazzari R, Vast N, Besson JM, Baroni S, Dal Corso A (1999) Phys Rev Lett 83(16):3230
- Pfrommer BG, Cote M, Louie SG, Cohen ML (1997) J Comput Phys 131(1):233
- Perdew JP, Burke K, Ernzerhof M (1996) Phys Rev Lett 77(18):3865
- Kobayashi M (1988) J Mater Sci 23(12):4392. doi:[10.1007/BF00551937](https://doi.org/10.1007/BF00551937)
- Katada K (1966) Jpn J Appl Phys 5(7):582
- Palatnik LS, Kozma AA, Nechitailo AA (1983) Kristallografiya 28(1):136
- Galasso F, Kuehl D, Tice W (1967) J Appl Phys 38(1):414
- Galasso F, Vaslet R, Pinto J (1966) Appl Phys Lett 8(12):331
- Werheit H, Leithe-Jasper A, Tanaka T, Rotter HW, Schwetz KA (2004) J Solid State Chem 177(2):575
- Shirai K, Emura S (1997) J Solid State Chem 133(1):93
- Shirai K, Emura S (1996) J Phys Condens Matter 8(50):10919
- Franz R, Werheit H (1989) Europhys Lett 9(2):145
- Morosin B, Kwei GH, Lawson AC, Aselage TL, Emin D (1995) J Alloy Compd 226(1–2):121
- Werheit H (2006) J Phys Condens Matter 18(47):10655
- Bao RQ, Yan ZJ, Chrisey DB (Unpublished data)
- Badzian AR (1967) Mater Res Bull 2(11):987